FEATURE ARTICLE

Molecular Simulation Analysis and X-ray Absorption Measurement of Ca^{2+}, K^+ and Cl^- Ions in Solution

Liem X. Dang,* Gregory K. Schenter, Vassiliki-Alexandra Glezakou, and John L. Fulton

Chemical Sciences Division, Pacific Northwest National Laboratory, Richland, Washington 99352

Received: July 22, 2006; In Final Form: October 5, 2006

This paper presents recent advances in the use of molecular simulations and extended X-ray absorption fine structure (EXAFS) spectroscopy, which enable us to understand solvated ions in solution. We report and discuss the EXAFS spectra and related properties governing solvation processes of different ions in water and methanol. Molecular dynamics (MD) trajectories are coupled to electron scattering simulations to generate the MD-EXAFS spectra, which are found to be in very good agreement with the corresponding experimental measurements. From these simulated spectra, the ion−oxygen distances for the first hydration shell are in agreement with experiment within 0.05−0.1 Å. The ionic species studied range from monovalent to divalent, positive and negative: K^+, Ca^{2+}, and Cl^-. This work demonstrates that the combination of MD-EXAFS and the corresponding experimental measurement provides a powerful tool in the analysis of the solvation structure of aqueous ionic solutions. We also investigate the value of electronic structure analysis of small aqueous clusters as a benchmark to the empirical potentials. In a novel computational approach, we determine the Debye−Waller factors for Ca^{2+}, K^+, and Cl^- in water by combining the harmonic analysis of data obtained from electronic structure calculations on finite ion−water clusters, providing excellent agreement with the experimental values, and discuss how they compare with results from a harmonic classical statistical mechanical analysis of an empirical potential.

1. Introduction

A molecular-level understanding of ion−water and water−water interactions in solvation processes is essential to understanding the chemical and physical properties and transport mechanism of ions in aqueous solutions. Molecular dynamics (MD) and Monte Carlo (MC) simulation techniques provide a powerful approach to probing such processes in condensed-phase environments.[1] Ab initio electronic structure calculations provide accurate predictions of geometries, energetic differences, and thermodynamic corrections, all of which are directly associated with the spectroscopy of the systems under study.[2]

A detailed description of the solvent structure around an ion in solution can be obtained from a variety of experimental and theoretical techniques. MD simulations provide a detailed picture of structure and dynamics for complex systems that may not be tractable by other methods. At the heart of a computational study are the potential functions that have been very successful in describing complex phenomena.[3] However, there is need for increasingly better accuracy to describe multiphase systems, interfaces, nanoscale materials, and processes such nucleation and ion solvation. It is important to show that the simulation not only reproduces important macroscopic properties but also the molecular structure and dynamics of the ions in real systems. In this respect, it is then possible to benchmark the performance of MD simulation by using (1) the highest level of theory possible in an electronic structure calculation of finite size clusters, and (2) spectroscopic studies of the hydrated ions in bulk solution from extended X-ray absorption fine structure (EXAFS) measurements.

We use a powerful combination of these three different techniques to determine the structure for several abundant aqueous ion species, Ca^{2+}, K^+, and Cl^-. Aqueous solutions of these light element ions are ubiquitous in nature. The interaction of these ions with water is responsible for a diverse number of chemical, geochemical, biochemical, and atmospheric chemistry processes.[4−8] As a logical extension of the comparison between different ions, we also explore the structure of solvated ions in methanol, another polar solvent with capability of forming hydrogen bonds. A significant contribution to this last subject is the work of Berendsen and co-workers on simulations of the EXAFS spectrum of dilute Sr^{2+} in liquid methanol.[9]

Due to the advance of modern EXAFS algorithms and the availability of more accurate ion and solvent potential models, the number of studies that combine MD with EXAFS has increased considerably.[10−51] Our work is distinguished from early contributions in that we combine MD, ab initio quantum chemical calculations and EXAFS measurement to address the ion solvation in aqueous solution. We have recently developed a method to predict EXAFS spectra: an ensemble of molecular configurations is generated from an intermolecular potential and is subsequently used in electron scattering analysis. For instance, McCarthy et al.[13,52] have reported a direct method to generate MD-EXAFS spectra from an MD simulation. This is an important outcome of an earlier contribution by Palmer et al.[53] This method obviates the need to compare poorly defined entities such as coordination or solvation numbers by a direct comparison of experimentally measured and simulated spectral

* Corresponding author.

10.1021/jp064661f CCC: $33.50
Published on Web 11/09/2006

Liem X. Dang was born in Hue, Vietnam. He came to the U.S. in 1975 as a Vientamese refugee. Liem received his B.S. with honors in Chemistry with a minor in Mathematics in 1980 from Florida Institute of Technology and his Ph.D. in Physical Chemistry in 1985 from the University of California at Irvine, under the guidance of Professor Max Wolfsberg. Liem has worked with Monte Pettitt of the University of Houston and with the late Peter Kollman of UCSF. Liem is currently a Chief Scientist at the Pacific Northwest National Laboratory. He has authored or co-authored or 80 peer-reviewed publications on the development and use of molecular dynamics computer simulation techniques to study molecular complex systems.

Gregory S. Schenter received his degree in Physics from California Institute of Technology and his Ph.D. in Applied Physics from Cornell University. He joined PNNL in 1988 and has been promoted to Chief Research Scientist since 1998. Dr. Schenter's research interests include method development for vapor-phase nucleation and quantum statistical mechanics of materials, clusters, and activated chemical reactions.

Vassiliki-Alexandra Glezakou received her Bachelor's degree in Chemistry from the National Kapodistrian University of Athens, Greece, and her Ph.D. in Physical and Theoretical Chemistry from Iowa State University under the guidance of Professor Mark S. Gordon. In 2001 she joined Professor Peter R. Taylor's group at University of California San Diego, and in 2003 she became Staff Scientist at California Institute of Technology. She joined PNNL in 2004 as a Staff Scientist. She is interested in the chemistry and spectroscopy of energetic materials, transition metals, and heavy elements and their compounds.

John Fulton received his M.S. in Chemical Engineering from the University of Washington in 1985. He is currently a Staff Scientist in the Chemical Sciences Division of Pacific Northwest National Laboratory. He has published over 100 papers dealing with the structure of multi-molecular aggregates in condensed phases under both ambient and extreme conditions. His research interests are focused on developing a molecular-level understanding of the effect of extreme pressure and temperature on the structure and dynamics of both ion/water and ion/ion interactions.

quantities. As Ferlat et al.[10] point out, the methods which take into account the atomic environment are the most appropriate for the study of disordered systems and MD methods are a particularly valuable tool in this respect, as they naturally lead to an effective way of testing intermolecular potentials that are used in simulations. The advantage of MD-EXAFS is that all details of the ion−water structure inherent in the simulations are represented in the MD-EXAFS spectrum. Thus, the generation of the MD-EXAFS spectrum contains no assumption about the form of the ion−water pair potential.

EXAFS is a method widely used for the characterization of solvent−solute interaction. In EXAFS, an X-ray source is tuned to energies just slightly above an inner-shell electron absorption edge. As a result, a low-energy electron is ejected and is back-scattered by atoms of the nearest solvent shells. This scattering process leads to interferences with the outgoing wave, giving rise to the characteristic oscillations of the EXAFS spectra. With the help of the present theory, the number and type of surrounding atoms, their average distance to the central absorbing atom, and their distribution about the absorbing center can be ascertained. A more complete understanding of the structural information contained in the EXAFS spectra has been derived in many instances from MD simulations of the aqueous system.[10−51] In standard EXAFS analysis, the fine structure factor is defined by

$$\chi(E) = \frac{\mu(E) - \mu_0(E)}{\Delta\mu_0(E_0)} \tag{1}$$

where $\mu(E)$ is the absorption coefficient as a function of the X-ray energy $E = E_0 + \hbar^2k^2/2m_e$, $\mu_0(E)$ is the background absorption coefficient, and $\Delta\mu_0(E_0)$ is the jump in the absorption background at the absorption edge, E_0. EXAFS spectra provide predictions of the number of water molecules in the first solvation shell, which is the average distance of these scatterers from the central atom, and a measure of the static disorder of this first solvation shell, as well as the vibrational disorder. The latter effectively corresponds to the Debye−Waller factors, which are incorporated in one of the terms of the EXAFS scattering expansion.

We employ an updated version of the efficient algorithm for evaluating the electron multiple scattering series by Rehr et al.[54] as it is implemented in the code FEFF8.[55] We also carry out direct comparison of the Debye−Waller factors from a harmonic

classical statistical mechanical analysis of an empirical potential to those from a harmonic quantum statistical mechanical analysis of results from converged electronic structure calculations. The purpose of this article is to summarize the progress made in recent years in molecular simulation analysis and experimental X-ray absorption measurement of solvated ions. In our paper we report the EXAFS spectra determined from MD simulations and experimental measurement and the physical quantities, which can be determined from them, such as the number of solvent molecules of the first solvation shell and the Debye−Waller factors. The latter is a particularly interesting quantity as it is directly associated to the local environment of the solvated ions and their interaction with the solvent molecules. An important and original contribution of this work is a computational procedure for determining the Debye−Waller factors through the integrated combination of MD simulations and electronic structure calculations.

2. Experimental details

NaCl (99.999%), $NaClO_4 \cdot H_2O$ (99%), KCl (99.999%), anhydrous $CaCl_2$ (99.99%), $Ca(ClO_4)_2 \cdot (H_2O)_4$ (99%), and anhydrous methanol (99.8%) were used as received from Aldrich. Distilled, deionized water was used throughout. The methanol solutions were prepared in an Ar-purged glove box to avoid contamination by moisture in the air. The dielectric constant of methanol (32.7) is substantially lower than that of water (80.1), hence methanol might be more prone to formation of Ca−Cl contact ion pairs that would complicate the interpretation of the solvated Ca^{2+} ion. Thus, for the $CaCl_2$/methanol solutions, a series of concentrations from 0.025, 0.2, and 2.9 m $CaCl_2$ were studied. The latter condition was at the saturation point of $CaCl_2$ in methanol. The $\chi(k)$ data for all three conditions were very similar, suggesting that the degree of contact ion pairing is small, even at the saturation condition. In an earlier study, we have shown that for 6.0 m $CaCl_2$ in water there are virtually no contact ion pairs. As a further measure, we also briefly examined a solution containing 0.025 m $Ca(ClO_4)_2 \cdot (H_2O)_4$ in methanol. Because of its much large size, the $(ClO_4)^-$ ion is known to be a relatively weak ion pair former. The spectra of the $Ca(ClO_4)_2$ solution were the same as that of the $CaCl_2$ solution, again indicating that the Cl^- is not forming ion pairs under the conditions of this study.

The beamline and sample handling methods for the Ca^{2+} and K^+ have been previously described in detail.[56,57] In the following section we describe the methods used for acquisition of the chloride *K*-edge (2822 eV) EXAFS spectra. Spectral data were collected on a bending magnet beamline (Sector 20) of the PNC/XOR facility at the Advanced Photon Source (APS), Argonne National Laboratory. For measurements of the 2.5 m NaCl solutions, approximately ten single 20-minute scans were co-added to obtain high-quality transmission spectra. The X-ray optics included a Ni-coated harmonic rejection mirror that achieves a high level of harmonic rejection.[56] Acquisition of Cl K-edge (3608.4 eV) is a particularly challenging problem, because of the strong X-ray absorption of the windows, which severely limits transmission. Experimental details about the method used can be found in our previously published work.[57] The liquid sample holder used in these studies has been previously described for studies of Ca^{2+} solutions.[56] In this method a very thin liquid layer is contained between two pieces of thin prolene film (isotactic polypropylene) that are stretched over a "U"-shaped Kapton spacer that defines the path length. The solution path length was set at 75 μm and the solution was contained between two, 4-μm-thick prolene windows. Spectra that were acquired at different path lengths and concentrations were identical, demonstrating that absorption effects did not distort the $\chi(k)$ data. In general, the absorption edge height, $\Delta\mu_0$, for these transmission measurements was below 2 in all cases, as required to eliminate X-ray leakage effects. In order to verify the accuracy of EXAFS amplitudes measured in the transmission measurements, the 2.5 m NaCl sample was also run in fluorescence mode using a standard 90° geometry. After applying a standard self-absorption correction, the amplitudes in the fluorescence and transmission were equivalent.

TABLE 1: Potential Parameters for Ca^{2+}, Cl^-, K^+, and H_2O Used in MD Simulations

molecule	atom	σ (Å)	ϵ (kcal/mol)	q (e)	α (Å^3)
H_2O	H	0.000	0.0000	0.5190	0.000
	O	3.234	0.1825	0.0000	0.000
	M	0.000	0.0000	−1.0380	1.444
K^+	K	3.047	0.1000	1.0000	0.830
Ca^{2+}	Ca	2.9132	0.1000	2.0000	0.470
Cl^-	Cl	4.3387	0.1000	−1.0000	3.690

3. Computational Details

3.1. MD Simulations. We employ the rigid-body polarizable water model of Dang and Chang[3] to describe the water−water intermolecular interaction. This model describes reasonably well the structure and thermodynamic properties of the bulk and the liquid/vapor interface of water. The total interaction energy of the system is summarized as follows:

$$U_{tot} = U_{pair} + U_{pol} \tag{2}$$

$$U_{pair} = \sum_i \sum_{j>i} \left(4\epsilon_{ij} \left[\left(\frac{\sigma_{ij}}{r_{ij}} \right)^{12} - \left(\frac{\sigma_{ij}}{r_{ij}} \right)^{6} \right] + \frac{q_i q_j}{r_{ij}} \right) \tag{3}$$

and

$$U_{pol} = -\sum_{i=1}^{N} \mu_i \cdot E_i^0 - \frac{1}{2} \sum_{i=1}^{N} \sum_{j=1, i \neq j}^{N} \mu_i \cdot \boldsymbol{T}_{ij} \cdot \mu_j + \sum_i^N \frac{|\mu_i|^2}{2\alpha_i} \tag{4}$$

Here, r_{ij} is the distance between site i and j, q is the charge, σ and ϵ are the Lennard-Jones parameters, E_i^0 is the electric field at site i produced by the fixed charges in the system, μ_i is the induced dipole moment at atom site i, and $\boldsymbol{T}_{ij}$ is the dipole tensor. The first term in eq 4 represents the charge−dipole interaction, the second term describes the dipole−dipole interaction, and the last term is the energy associated with the generation of the dipole moment μ_i. During molecular dynamics simulations, a standard iterative self-consistent field procedure is used to evaluate the induced dipoles. The potential parameters used in the MD simulations for the aqueous solutions of Ca^{2+}, K^+, and Cl^- are listed in Table 1. The ion−water potential parameters were taken from our early work and were obtained by running molecular dynamics simulations to reproduce experimental data such as solvation enthalpies and hydration numbers, as well as the data reported from accurate electronic structure calculations for the clusters.[57]

3.2. EXAFS and MD-EXAFS Analysis. All $\chi(k)$ data were weighted by k^3 and windowed between $2.0 < k < 9.5$ Å^{-1} using a Hanning window[54] $W(k)$ with $dk = 1.0$ Å^{-1} (see later discussion). In general, the contribution from second and higher

hydration shells has negligible effect on the measured or simulated $\chi(k)$ spectra because the distances and the disorder are too large. For the experimental spectrum of potassium, inclusion of K−H, K−O−H, or K−O−O scattering paths did nothing to improve the quality of the fits. On the contrary, for chloride, both the Cl−O single scattering path and the Cl−H−O focusing path were the most significant contributions to the scattering signal. In order to estimate the core−hole factor, S_0^2, we used finely ground KCl in an inert hydrocarbon, while for chloride, a solution of 2.5 m $NaClO_4$ in the liquid sample holder with the 75 μm path length. The S_0^2 value was then found to be 0.98 for KCl and 0.92 for $CaClO_4$. The latter system was then used for estimating the coordination numbers for the 2.5 m NaCl solution. Uncertainties in the experimental estimate of S_0^2 lead to an error of approximately 20% in the reported coordination numbers in both systems.

For both K^+ and Cl^- aqueous systems, in which there is a higher degree of disorder in the first solvation shell, the EXAFS oscillations are relatively weak, and contributions from weak multi-electron excitations[56−57] represent a larger proportion of the total absorption intensity. There are several multi-electron excitations that are removed using methods similar to those previously described.[56] These excitations occur at $k = 2.6$, 3.4, and 9.6 Å^{-1} for K^+, and $k = 2.0$, 2.8, and 8.1 Å^{-1} for Cl^-, each set of numbers corresponding to the $KM_{II,III}$, KM_I, and $KL_{II,III}$ and transitions, respectively. The same series of excitations with similar edge-step magnitudes are clearly evident in the spectrum of K(0) vapor, Ar gas, and HCl gas. Our strategy for efficient removal is to first fit the general multi-electron background features of Ar and pure HCl gas with an arctan function ($KM_{II,III}$, $KL_{II,III}$) and with an arctan+slope change function (KM_I). The fitting of the K^+/H_2O and Cl^-/H_2O structural parameters was compared both with and without removal of the multi-electron features. All Cl *K*-edge EXAFS spectra contained a small contribution from the Ar *K*-edge at $k = 10.0$ Å^{-1}, even though extensive experimental efforts were employed to reduce its contribution. This artifact was also removed by fitting and subtracting an arctan function. The Ar *K*-edge occurs significantly beyond the detectable oscillations, and hence removing this artifact only aided the background removal process.

3.3. Electronic Structure Calculations. Finite-size cluster calculations were performed on the following systems: $Ca[H_2O]_n^{2+}$, $n = 1-8$; $K[H_2O]_n^+$, $n = 1-7$; and $Cl[H_2O]_n^-$, $n = 1-6$ at the aug-cc-CVpVDZ/MP2 level of theory.[58−60] Our structures are in accordance with previous detailed studies on these systems.[61−64] Although more than one minima are often taken into account in our approach, inclusion of all possible minima is beyond the scope of this work, and therefore only the most stable ones are included. All structures were fully optimized, and the harmonic frequencies were obtained by numerical difference of the analytic gradients at the same level, and subsequently scaled by the appropriate scaling factor for the method used, in this case 0.96.[65] All calculations were performed with the GAMESS suite of codes.[66] As it will be discussed in the following section, the frequencies are directly related to the Debye−Waller factors and are convoluted with the radial function distribution of the first peak corresponding to the M−O distance for the first solvation shell in order to obtain a very good estimate of this quantity.

4. Results and Discussion

4.1. MD-EXAFS Spectra. MD-EXAFS spectra can be produced through molecular simulation. Once the empirical potential is constructed, an ensemble average is generated using statistical mechanics simulation techniques. With the explicit representation of atomic positions corresponding to the molecular structure, one can generate the radial distribution function, $g(R)$. The radial distribution functions for Ca^{2+}, K^+, and Cl^- in water are shown in Figure 1. The dynamics of exchange in the first hydration shell of a solvated ion are characterized by the potential of mean force, $w(R)$. In this case the reaction coordinate is the ion−oxygen distance and the effective potential of the mean force is related to the radial distribution function, $g(R)$ as follows:

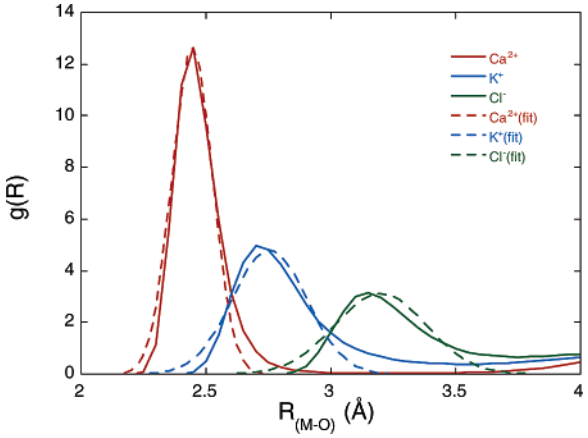

Figure 1. Radial distribution functions for aqueous solutions of Ca^{2+}, K^+, and Cl^- at 300 K. Dashed lines are the results due to the fits to a Gaussian distribution.

$$\exp(-\beta w(R)) = 4\pi R^2 g_{MO}(R) \tag{5}$$

where $4\pi R^2 g_{MO}(R)$ is the probability of finding the oxygen O of a water molecule within the interval (R, R+dR) from the solute M. The magnitude of this potential is associated with the binding interactions of the nearest solvent molecules with the solute. The minimum of the potential corresponds to the mean distance of the solvent molecules from the solute. The curvature is a measure of the "stiffness" of this mean interaction and is related to the fluctuations about this mean distance. We find that the curvature is dominated by only a few symmetric and antisymmetric stretches of the solute−solvent motions.

In the current work we will analyze the characteristics of the first peak of the radial distribution function, Figure 1. In each of these simulations, we used a Gaussian distribution to fit the first peak of the radial distribution function as demonstrated in Figure 1:

$$\rho_0 4\pi R^2 g(R) \approx \frac{N_0}{\sqrt{2\pi\sigma_G^2}} e^{-[(R-R_0)^2]/2\sigma_G^2} \tag{6}$$

The coordination number, N_0 determines the normalization and ρ_0 is the water number density. The mean position, R_0, and variance or Debye−Waller factor, σ_G^2, effectively characterize the peak. In some systems the Debye−Waller factor as determined from the simulation can be considerably different from the "ideal" Gaussian width. As seen from Figure 1, the fit provides a reasonable representation of the first solvent shell. This correspondence enables us to approximate the coordination number, N_0, through a straightforward fit. In Table 2, we summarize these parameters obtained from molecular simulation using the empirical potentials.

EXAFS is a decidedly short-range technique when compared to competing methods such as X-ray and neutron scattering.

TABLE 2: Parameters Characterizing the First Peak of the Radial Distribution Function Determined from MD

ion	R_0 (Å)	σ^2 (Å^2)	N
Ca^{2+}	2.45	0.0066	6.5
K^+	2.77	0.0221	5.7
Cl^-	3.22	0.0334	6.2

TABLE 3: Parameters Characterizing the First Peak of the Radial Distribution Function Determined from Analysis of Measured EXAFS Spectra[a]

ion	R_0(Å)	σ^2(Å)	N
Ca^{2+}	2.429	0.0115	6.8
K^+	2.732	0.0293	6.1
Cl^-	3.110	0.0290	6.4

[a] Typical uncertainties for all cases for R_0 and N are ±0.03 Å and ±1.0 Å, respectively. For K^+ and Cl^-, σ^2 is ±0.004 Å^2 whereas for Ca^{2+} σ^2 is ±0.002 Å^2.

The advantage of EXAFS over other scattering methods is that the scattered photoelectron emanates from the core of the ion of interest and is not convoluted with scattering from other types of ions or from water−water interactions. This simplifies enormously the interpretation of the data. In aqueous solutions, numerous studies have confirmed that the scattering originates almost exclusively from the oxygen of the water in the first shell. A shortcoming of this method with respect to other scattering methods is that the higher shell structure, especially the second hydration shell, is not resolved. However, as we will show, the high quality information from the first shell is sufficient for evaluation of MD potential models and for comparison with small clusters generated from electronic structure calculations. Finally, the EXAFS measurements can be made under very low concentrations where ion−ion interactions are negligible, thus providing the most accurate determination of ion hydration structure.

An analysis of the relation between EXAFS spectra and molecular structure has benefited from the availability of efficient algorithms for the evaluation of electron scattering analysis such as those implemented in the FEFF8 code by Rehr, Albers, and Zabinsky.[54] The average EXAFS spectrum is obtained from a configurationally average

$$\bar{\chi}(E) = \frac{\bar{\mu}(E) - \mu_0(E)}{\Delta\mu_0(E_0)} \tag{7}$$

where bars denote the said configurational average. This is often fitted to the expression

$$\bar{\chi}(k) = \sum_i N_i S_0{}^2 \frac{\bar{F}_i(k)}{k\bar{R}_i{}^2} e^{-2\bar{R}_i/\lambda - 2k^2\sigma_i{}^2} \sin\left[2k\bar{R}_i + \bar{\varphi}_i(k) - \frac{4}{3}C_{3,i}k^3\right] \tag{8}$$

In this expression, $\bar{F}_i(k)$ is often estimated from a single symmetric characteristic configuration and is assumed to have insignificant fluctuations with configuration. The Debye−Waller factor, $\sigma_i{}^2$, and the third cumulant, $C_{3,i}$, reflect the structural disorder of the system. In Table 3 we display results from fitting the expression given by eq 8 to measured EXAFS spectra. A comparison of simulated results in Table 2 to measured results corresponding to Table 3 reveals that R_0 estimates are consistent to within 0.1 Å. For the cations, the Debye−Waller factors determined from simulation are significantly smaller than those determined from analysis of EXAFS measurements. Further comparison between measurement and simulation is provided by the MD-EXAFS procedure in which an ensemble of configurations is generated by an empirical potential. Electron scattering analysis is then performed on each configuration to generate an individual fine structure spectrum. These spectra are finally averaged to obtain the fine structure corresponding to the simulation and the empirical potential.

Figures 2a−c show the k^2-weighted $\chi(k)$ plots of aqueous Ca^{2+}, K^+, and Cl^-, and Figure 3 the corresponding plot of Ca^{2+} in methanol at 300 K, from experiment and MD-EXAFS simulations. Consistent with Tables 2 and 3, the wavelength of the oscillations with respect to k appears to match between experimental measurement and MD-EXAFS, confirming that the mean distances are in agreement. Experimental measurements indicate that the decay of the envelope of oscillations is shorter in k for Ca^{2+} and K^+ than the value predicted by MD-EXAFS, which translates to smaller Debye−Waller factors in the latter case.

In order to obtain a real-space representation of the EXAFS spectra, we calculated the Fourier transform of the structure factor as implemented in the FEFFIT package,[54] where $W(k)$ is a Hanning window:

$$\tilde{\chi}(R) = \frac{1}{\sqrt{2\pi}}\int_0^\infty k\chi(k)W(k)e^{i2kR}\,dk \tag{9}$$

Experimental and simulated spectra were transformed in an identical manner for direct comparison. As a result, $\tilde{\chi}$(R) reduces to a series of peaks centered at the atomic distances, R_i, in the limit that $F_i(k)$ and $\varphi_i(k)$ do not depend on k. Aside from the distortion due to electron scattering and phase shift described in eq 9, $\tilde{\chi}(R)$ is a direct measurement of the radial probability, $4\pi R^2 g(R)$ in the region of the first solvation shell. Comparison of experimental results to MD-EXAFS for aqueous Ca^{2+}, K^+, and Cl^-, and Ca^{2+} in methanol at 300 K is shown in Figures 4a−c and 5 respectively, from which it is evident that the peak positions are consistent between experimental measurement and MD-EXAFS. It is also apparent that the experimental values of the peak widths of the cations studied here are larger than the corresponding values of the MD-EXAFS simulations, both in water and methanol. For Cl^-, the MD-EXAFS values are smaller than the experimental ones. This is consistent with the initial analysis.

Both water and methanol develop extensive networks of hydrogen-bonded molecules in the liquid phase. Whereas water is capable of up to four hydrogen bonds with its neighbors, methanol can be involved in two such interactions at most. The relatively simple, yet analogous, structure of methanol provides for an interesting way to compare the first shell solvation structure about Ca^{2+}. This allows us to assess the factors that govern the first shell structure in bulk solution.

In an earlier paper, intermolecular potential models for Ca^{2+} in methanol were reported from which an MD-EXAFS spectrum was generated.[67] In Figure 3, this MD-EXAFS $k^2\chi(k)$ plot is compared to experimental spectrum for a 0.2 m $CaCl_2$ solution in methanol at 300 K. As is the case for Ca^{2+}−water interaction (Figure 1), the MD simulation faithfully reproduces the major features of the spectrum. This is further demonstrated by the $|\tilde{\chi}(R)|$ plots in Figure 5 showing the real-space representation from the Fourier transformed $k^2\chi(k)$ data in Figure 3. In all cases, the primary peak in the $|\tilde{\chi}(R)|$ is from the Ca−O scattering from first-shell O's on water or methanol. The MD-EXAFS peak is narrower than for the experimental one for both water and methanol, indicating that the solvent molecules are more ordered about the Ca^{2+} in the simulated structures. There is little or no evidence of Ca−C scattering from the $-CH_3$ on the methanol in either the experiment or the simulation. This means that the

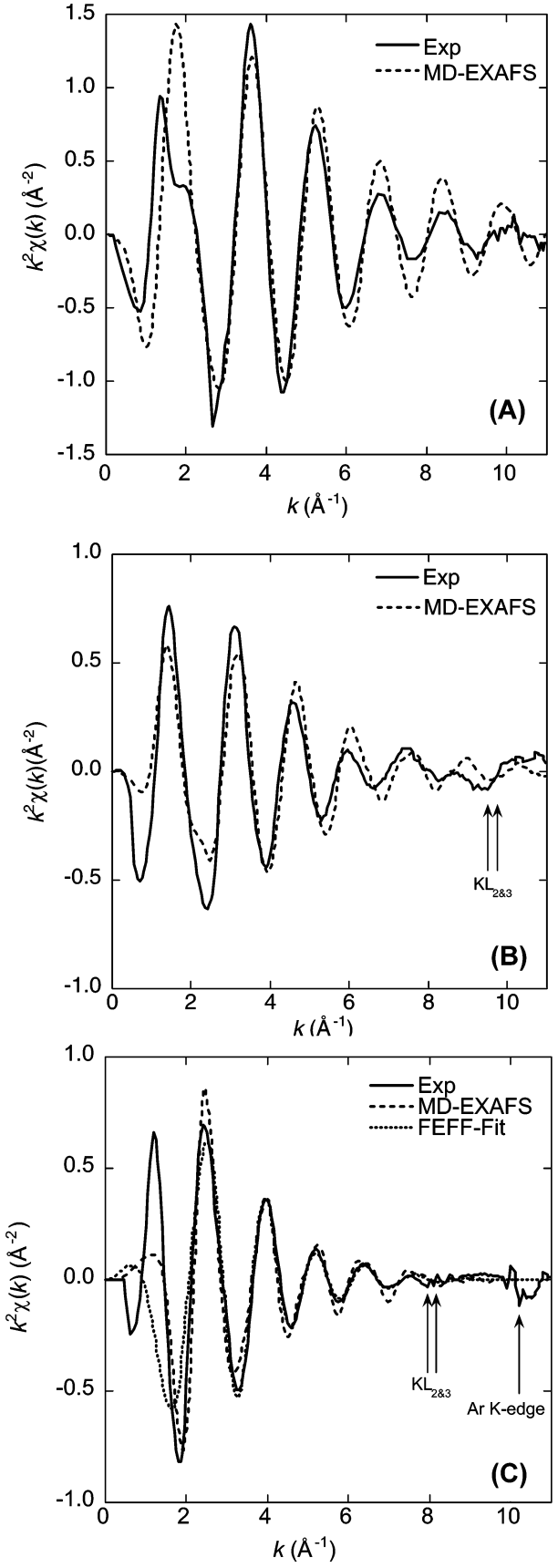

Figure 2. (a−c) Comparison between the structural factor for Ca^{2+} (2a), K^+ (2b), and Cl^- (2c) in water and the corresponding experimental measurements. We have also included the FEFF fit in Figure 2c.

wagging or rocking motions about the Ca−O−C bonds induce a large amount of positional disorder for the Ca−C distance,

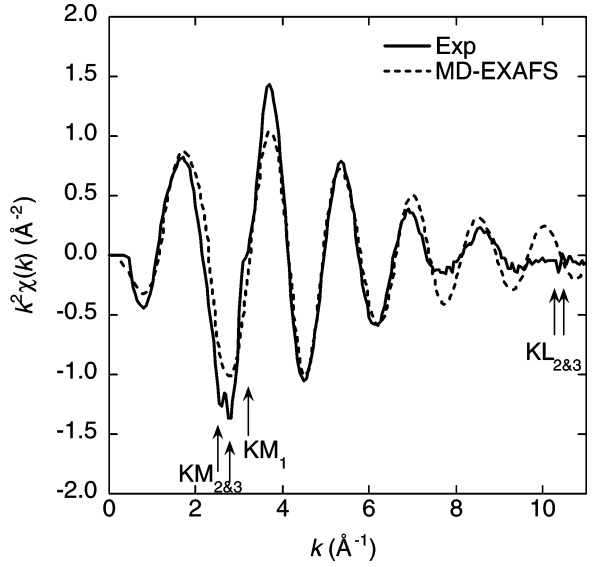

Figure 3. Comparison of the structural factor for Ca^{2+} in methanol from MD-EXAFS and experiment.

thereby dampening this contribution to the EXAFS signal. The higher degree of disorder is similar to that observed for Sr^{2+} in methanol, where the Sr−C scattering shows only very weak contribution to the total signal.[9]

Table 4 summarizes the average structural parameters derived from the RDF of the simulation and from EXAFS spectrum. It is also useful to compare the experimental (EXAFS) structure for Ca^{2+} in water to that in methanol. In all aspects, the spectra are nearly identical, within the experimental error: (i) the Ca−O distance is 2.43 Å in water vs 2.41 Å in methanol; (ii) the coordination number is 6.8 in water vs 6.9 in methanol; (iii) the Debye Waller factor is 0.0115 Å^2 in water vs 0.0118 Å^2 in methanol.

It is remarkable that although the $-CH_3$ group on the methanol impedes interaction with the second shell molecules it seems to have little effect on the first solvation shell structure. Even though methanol has a reduced capacity for hydrogen bonding within the second hydration shell compared to water, the structure of the first shell is nearly identical in the two environments. This observation explains the very good agreement between experiment and electronic structure calculations on small ion−solvent clusters: the small clusters examined by electronic structure do not include a second shell, and yet the disorder calculated for the first shell can be used to accurately determine the bulk solution value, because the disorder in the first shell is dominated by the Ca−O interactions and not by second shell interactions.

4.2. Cluster Analysis. It is reasonable to apply an empirical potential to a cluster system. When a full anharmonic, classical statistical mechanical sampling is applied to the system, the enthalpy of cluster formation compares favorably with experimental results,[68] as shown in Figures 6 and 7. The empirical potential was constructed to be consistent with classical statistical mechanical sampling, while the electronic structure results, within the Born−Oppenheimer approximation, are consistent with quantum statistical mechanical sampling of the nuclear degrees of freedom. The difference in sampling is emphasized by displaying the enthalpy of formation as a function of temperature. The difference between the empirical potential and the electronic structure results at $T = 0$ K is dominated by zero-point energy effects. As the temperature increases, quantum

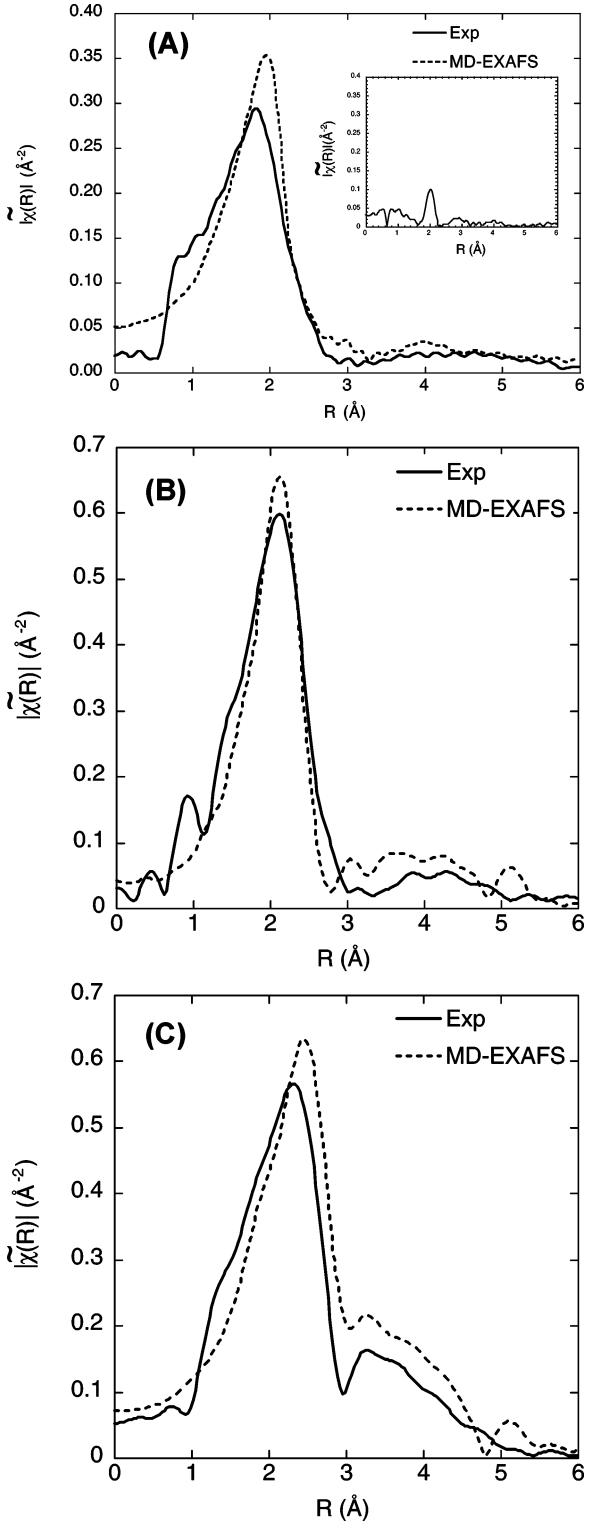

Figure 4. (a−c) Comparison between the MD-EXAFS spectrum for Ca^{2+} (4a), K^+ (4b), and Cl^- (4c) in water and the corresponding experimental measurements. We have also included in Figure 4a the difference in the intensity between the MD and the measurement, to illustrate the accuracy of approaches.

statistical mechanical effects become less important while anharmonicity effects become more significant. For a given cluster, it is possible to directly compare the Debye−Waller factor from a harmonic classical statistical mechanical analysis of an empirical potential to a harmonic quantum statistical mechanical analysis of results from converged electronic structure analysis.

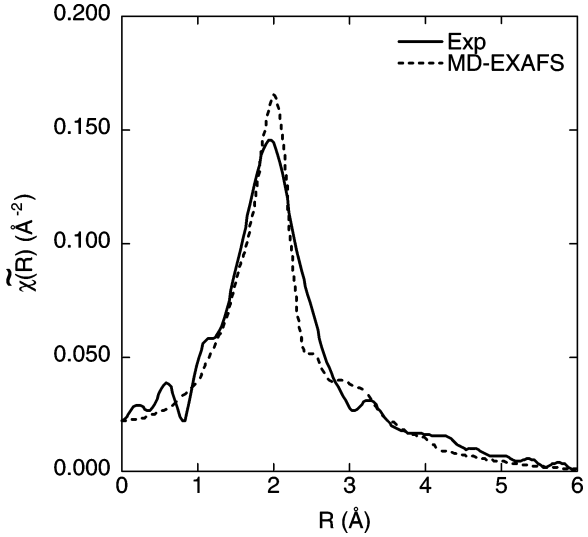

Figure 5. Comparison of the MD-EXAFS spectrum with experiment for Ca^{2+} in methanol.

TABLE 4: Parameters Characterizing the First Peak of the Radial Distribution Function for Ca^{2+} in Liquid Methanol as Determined from Molecular Simulation and from Analysis of Measured EXAFS Spectra

	R_0 (Å)	σ^2 (Å^2)	N
MD	2.400	0.0048	6.0
EXAFS	2.410	0.0118	6.9

We wish to understand the difference between the measured and calculated values of Debye−Waller factors. As a benchmark for evaluation of potentials, we will consider molecular clusters of the general formula $M[H_2O]_n^q$, where n is usually 1−8. Such systems have the advantage that they are small enough for electronic structure analysis to be performed and recover accurate interaction energies and harmonic frequencies. Subsequently, a direct comparison can be made between these results and the empirical potential results. The Debye−Waller factor relates directly to the harmonic frequencies by the formula

$$\sigma^2 = \sum_i \left(\frac{\partial R}{\partial z_i}\right)^2 \frac{k_B T}{\omega_i^2} \tag{10a}$$

where $(\partial R/\partial z_i)$ is the change of the normal coordinate i along the z direction, k_B is the Boltzmann factor, T the temperature, and ω_i the harmonic frequency of corresponding to normal coordinate i of a cluster cluster geometry produced by either MD simulation or quantum mechanical geometry optimization. In the latter case, the frequencies are further corrected for nuclear quantum mechanical effects and eq 10a becomes

$$\sigma^2 = \sum_i \left(\frac{\partial R}{\partial z_i}\right)^2 \frac{4k_B^3 T^3 \tanh^2\left(\frac{\hbar\omega_i}{2k_B T}\right)}{\hbar^2 \omega_i^2} \tag{10b}$$

There is a strong dependence of the Debye−Waller factors on the cluster size, as demonstrated in Figure 8 for the Ca^{2+}-$(H_2O)_n$ system, where $n = 1-6$. The K^+− and Cl^-−water clusters exhibit a similar dependence as well. In the same figure, the black line represents the EXAFS experimental measurement and the red one the bulk result obtained from the simulation using the classical empirical potential. We find that the harmonic electronic structure results are consistently higher than the

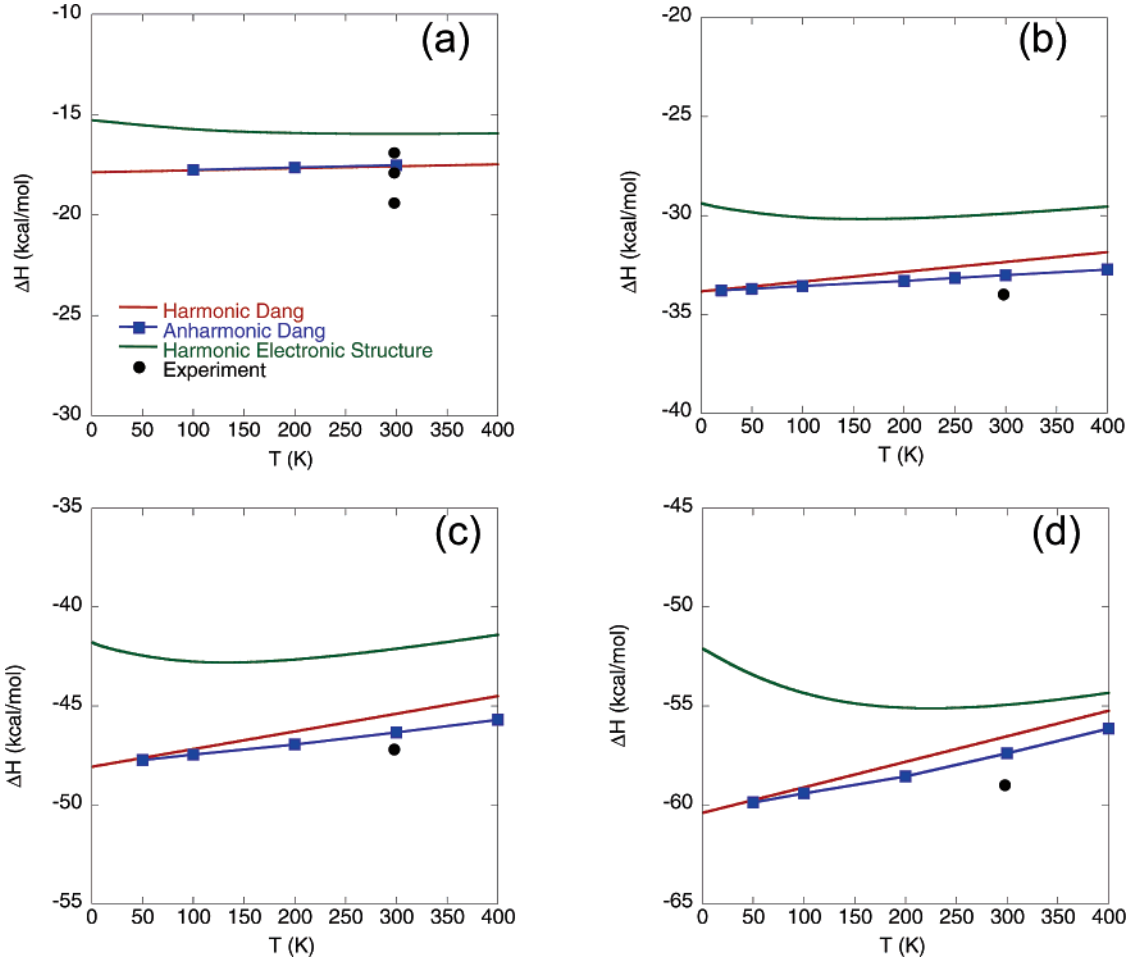

Figure 6. Temperature dependence of enthalpy of formation for $K^+-(H_2O)_{1-4}$ clusters in (a−d), respectively. Experimental values taken from ref 68.

harmonic results using the empirical potential, as shown in Figures 9a−c. While it is obvious that larger clusters approach the value for bulk measurements and are consistently better than the empirical simulation results, a well-defined relation between the cluster results and the bulk results is not straightforward, and the connection of cluster-size n to the bulk is not simple. Inclusion of anharmonicity has very little effect on the Debye−Waller factors for water-solvated Ca^{2+}, K^+, but starts becoming more important in the case of Cl^-, see Figure 10, indicating that for strongly solvated systems, the harmonic analysis provides a good estimate of the Debye−Waller factor. Anharmonicity also becomes more significant as the cluster size increases. Furthermore, for small n, a single minimum in the potential energy surface usually dominates, but this ceases to be the case as the clusters become larger.

In our effort to extract as much information as possible from the electronic structure calculations, we consider the correlation between the ion-oxygen distance and the corresponding harmonic Debye−Waller factor. As is evinced in Figures 9 and 10, when plotted as a function of ion−oxygen distance, the Debye−Waller factors exhibit some common characteristics, regardless of ion or charge: (a) the empirical potential results are systematically lower than the electronic structure results, and (b) on a logarithmic scale, there appears to be a common correlation between the ion−oxygendistance and the magnitude of the Debye−Waller factor. We find that the harmonic analysis recovers a "universal" dependence between the Debye−Waller factor and R, even though the curve is shifted toward smaller distances. We take advantage of this unique property by fusing results from electronic structure calculations with empirical potential simulations. As a first step, we establish the Debye−Waller factor dependence on R from electronic structure, $\sigma_{ES}^2(R)$ by fitting the natural logarithm of the Debye−Waller data accumulated from quantum calculations of small clusters into a simple linear function. In the next step, we obtain the radial distribution function from MD simulation of the empirical potential, $g_{MD}(R)$ and we combine the two results by integrating over the area on the first peak, which effectively corresponds to the average size for the first solvation shell, while the peak position corresponds to the average radius of the first solvation shell. In this way, we are able to recover an improved estimate of the Debye−Waller factor, noted as ES-MD:

$$\frac{1}{\ln(\sigma^2_{ES-MD})} = \frac{\int_0^{R_{min}} dR \, \frac{1}{\ln(\sigma^2_{ES}(R))} 4\pi R^2 g_{MD}(R)}{\int_0^{R_{min}} dR \, 4\pi R^2 g_{MD}(R)} \quad (11)$$

The results of this computational scheme are compiled in Table 5 and reveal a significant improvement of the ES-MD results over the one obtained simply with the empirical potential when compared to EXAFS measurement. For the cations, MD simulations predict 0.0066 and 0.0221 Å^2 for Ca^{2+} and K^+, compared to 0.0115 and 0.0293 Å^2, underestimating the Debye−Waller factor by 40% and 25% respectively. In the case of the anion Cl^-, MD simulations predict a higher value than the

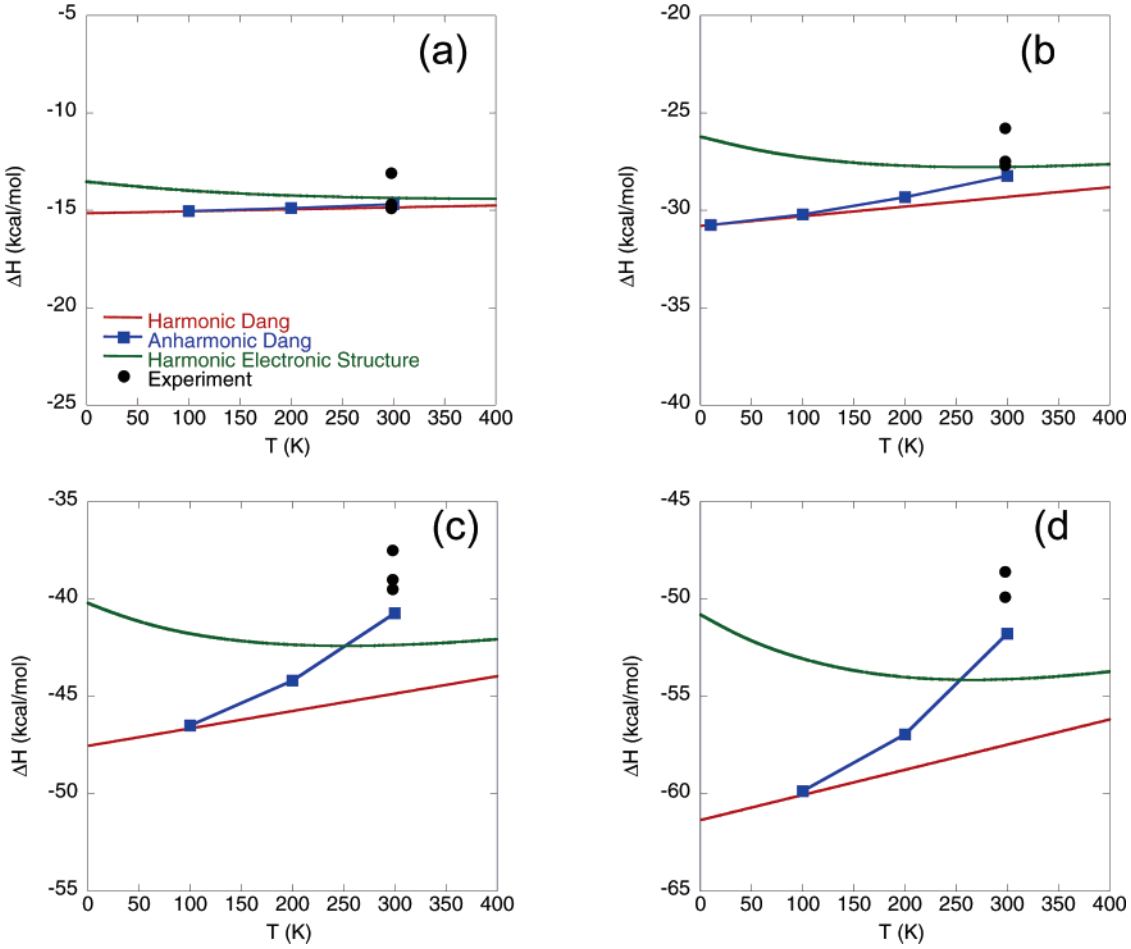

Figure 7. Temperature dependence of enthalpy of formation for $Cl^-(H_2O)_{1-4}$ clusters in (a−d), respectively. Experimental values taken from ref 68.

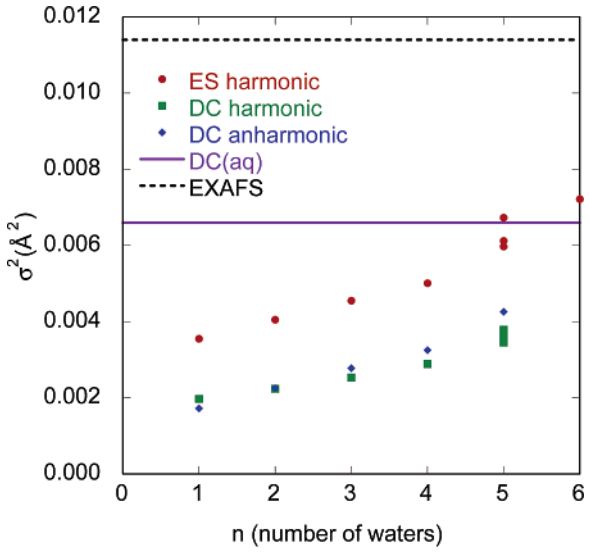

Figure 8. Cluster analysis (1−6 water molecules) of Debye−Waller factors from MD simulation (Dang-Chang polarizable potential), ab initio quantum-corrected calculations, and EXAFS at 300 K.

experimental one, 0.0334 compared to 0.0290 Å^2, overestimating it by 15%. When we combine electronic structure and MD, as shown in eq 11, the calculated values of the Debye−Waller factors for Ca^{2+} K^+, and Cl^- are 0.0107, 0.0276, and 0.0271 Å^2, respectively, and they are all consistently lower than the measured experimental values by only about 6%. We note here that the proposed rescaling of the MD Debye−Waller factors can be useful only for an ionic system with a weak interaction between the first and second hydration shell.

5. Conclusions and Outlook

We report a combined theoretical and experimental approach to describe and interpret the behavior of hydrated ions in gas and condensed phase. Using classical MD techniques and polarizable potential models, we present a detailed study of the solvation structure of Ca^{2+}, K^+, and Cl^- in water, as well as Ca^{2+} in methanol. We develop a set of polarizable ion−solvent interactions that accurately describes the hydration enthalpy, the coordination numbers, and the peak locations of the ion−solvent RDFs. Subsequently, MD EXAFS spectra are calculated and these are in good agreement with corresponding experimental measurements. Ab initio calculations are performed at a correlated level with augmented basis sets to locate equilibrium structures of ion−water clusters of variable size, and compute the Debye−Waller factors, a measure of the disorder in the solute's immediate environment, within the harmonic approximation. These two different modeling techniques are successfully combined in our novel approach of interfacing molecular dynamics with high-level, electronic structure cluster calculations to obtain a theoretical expectation value for the Debye−Waller factors. While MD-simulated EXAFS spectra underestimate the Debye−Waller factor, the ab initio−MD hybrid approach for the evaluation of EXAFS parameters is in excellent agreement with the experimental data.

In this work we employ polarizable potential models for the simulation of EXAFS spectra. The advantage of a simulation approach is that we are describing the molecular system directly.

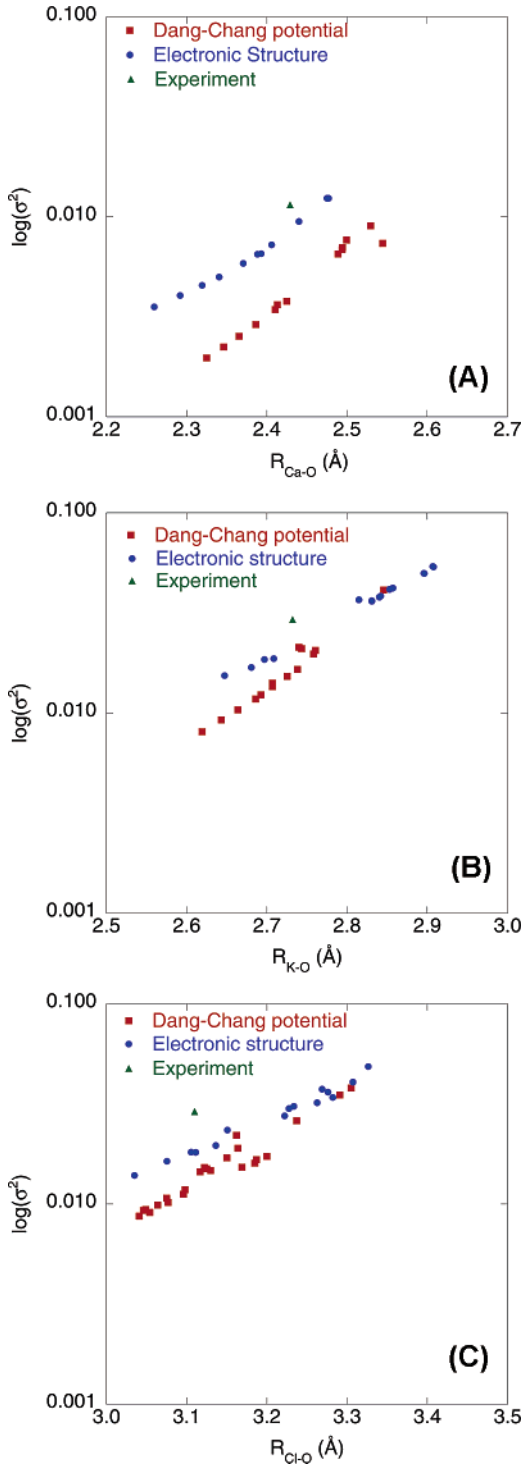

Figure 9. (a−c) Cluster harmonic analysis of Debye−Waller factors from MD simulation (Dang-Chang polarizable potential), ab initio quantum-corrected calculations and EXAFS at 300 K, for Ca^{2+}−water (9a), K^+−water (9b), and Cl^-−water (9c).

Sampling techniques exist so that we can generate *ensembles* of molecular configurations corresponding to temperature and density with confidence. The resulting description of the collective response of the solvent to the solute is only as good as the intermolecular potential. One advantage of the empirical potential approach is that we can use the same description of intermolecular interactions to describe the ion both in bulk and in discrete clusters. Furthermore, we can directly assess the role of anharmonicity by comparing harmonic models to fully anharmonic systems. We have therefore provided a detailed description of the structures of solvated ions at a molecular level. Obtaining this information through simulation is an initial step in developing first-principle predictions of transport mechanisms in complex molecular systems.

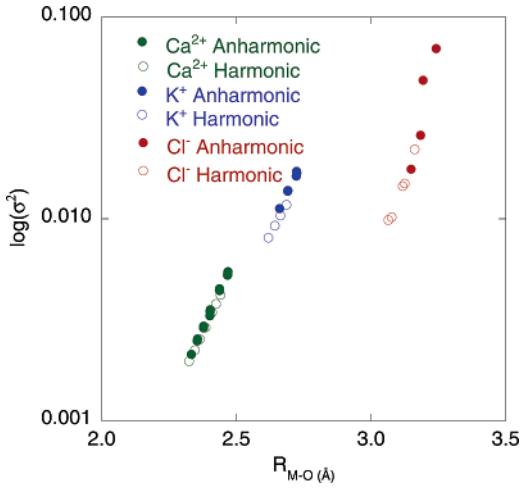

Figure 10. Anharmonic effects on cluster analysis of Debye−Waller factors from MD simulations (Dang-Chang polarizable potential).

TABLE 5: Debye-Waller Factors Obtained from MD, ES-MD and Measured EXAFS (Exp) in Water

	σ^2 (Å^2)		
	MD	ES-MD	exp
Ca^{2+}	0.0066	0.0107	0.0115
K^+	0.0221	0.0276	0.0293
Cl^-	0.0334	0.0271	0.0290

Acknowledgment. Work was supported by the Office of Science, Office of Basic Energy Sciences, Chemical Sciences Division of the U.S. Department of Energy (DOE). The Pacific Northwest National Laboratory is operated by Battelle for DOE. PNC/XOR facilities at the Advanced Photon Source, and research at these facilities, are supported by the U.S. DOE Office of Science Grant No. DEFG03-97ER45628, the University of Washington, a major facilities access grant from NSERC, Simon Fraser University and the Advanced Photon Source. Use of the Advanced Photon Source is also supported by the U.S. Department of Energy, Office of Science, Office of Basic Energy Sciences, under Contract No. W-31-109-Eng-38. The authors wish to thank Dr. John Daschbach and Dr. C. Wick for their insightful comments.

References and Notes

(1) Allen, M. P.; Tildesley, D. J. *Computer Simulation of Liquids*; Oxford University: Oxford, 1987.
(2) Feller, D. *J. Phys. Chem.* **1997**, *101*, 2723.
(3) Dang, L. X.; Chang, T.-M. *J. Chem. Phys.* **1997**, *106*, 8149.
(4) Haag, W. R.; David Yao, C. C. *Environ. Sci. Technol.* **1992**, *26*, 1005.
(5) Stadtman, E. R. *Annu. Rev. Biochem.* **1993**, *62*, 797.
(6) Halliwell, B.; Gutteridge, J. H. C. *Free Radicals in Biology and Medicine*; Oxford University Press: Oxford, 1989.
(7) Finlayson-Pitts; Pitts, B. J. *Chemistry of the Upper and Lower Atmosphere: Theory, Experiments, and Application*; Academic Press: New York, 2000.
(8) Wayne, R. P. *Chemistry of Atmospheres*; Oxford University Press: Oxford, 2000.
(9) Roccatano, D.; Berendsen, H. J. C.; D'Angelo, P. *J. Chem. Phys.* **1998**, *108*, 9487.
(10) Ferlat, G.; San Miguel, A.; Jal, J.-F.; Soetens, J.-C.; Bopp, P. A.; Daniel, I.; Guillot, S.; Hazemann, J.-L. and Argoud, R. *Phys. Rev. B* **2001**, *63*, 134202.
(11) Ferlat, G.; San Miguel, A.; Soetens, J.-C.; Bopp, P. A. *High Pressure Res.* **2002**, *22*, 399.

(12) Ferlat, G.; SanMiguel, A.; Jal, J.-F.; Soetens, J.-C.; Bopp, P. A.; Hazemann, J.-L.; Testemale, D.; Daniel, I. *J. Mol. Liq.* **2002**, *101*, 127.
(13) McCarthy, M. I.; Schenter, G. K.; Chacon-Taylor, M. R.; Rehr, J. J.; Brown, G. E. *Phys. Rev. B* **1997**, *567*, 9925.
(14) Roccatano, D.; Berendsen, H. J. C.; D'Angelo P. *J. Chem. Phys.* **1998**, *108*, 9487.
(15) Hoffmann, M. M.; Darab, J. G.; Palmer, B. J.; Fulton, J. L. *J. Phys. Chem. A* **1999**, *103*, 8471.
(16) D'Angelo, P.; Di Nola, A.; Filipponi, A.; Pavel, N. V.; Roccatano, D. *J. Chem. Phys.* **1994**, *100*, 985.
(17) D'Angelo, P.; Di Nola, A.; Giglio, E.; Mangoni, M.; Pavel, N. *J. Phys. Chem.* **1995**, *99*, 5471.
(18) D'Angelo, P.; Di Nola, A.; Mangoni, M.; Pavel, N. *J. Chem. Phys.* **1996**, *104*, 1779.
(19) D'Angelo, P.; Nolting, H.-F.; Pavel, N. *Phys. Rev. A* **1996**, *53*, 798.
(20) D'Angelo, P.; Pavel, N.; Roccatano, D.; Nolting, H.-F. *Phys. Rev. B* **1996**, *54*, 12129.
(21) D'Angelo, P.; Pavel, N. *J. Chem. Phys.* **1999**, *111*, 5107.
(22) D'Angelo, P.; Pavel, N. *J. Synchrotron Radiat.* **1999**, *6*, 281.
(23) D'Angelo, P.; Pavel, N. *J. Synchrotron Radiat.* **2001**, *8*, 173 and references therein.
(24) D'Angelo, P.; Barone, V.; Chillemi, G.; Sanna, N.; Meyer-Klaucke, W.; Pavel, N. *J. Am. Chem. Soc.* **2002**, *124*, 1958.
(25) Chillemi, G.; D'Angelo, P.; Pavel, N. V.; Sanna, N.; Barone, V. *J. Am. Chem. Soc.* **2002**, *124*, 1968.
(26) Filipponi, A.; Di Cicco, A. *Phys. Rev. B* **1995**, *51*, 12322.
(27) Di Cicco, A. *J. Phys.: Condens. Matter* **1996**, *8*, 9341.
(28) Di Cicco, A.; Rosolen, M. J.; Marassi, R.; Tossici, R.; Filipponi, A.; Rybicki, J. *J. Phys.: Condens. Matter* **1996**, *8*, 10779.
(29) Di Cicco, A.; Minicucci, M. *J. Synchrotron Radiat.* **1999**, *99*, 255.
(30) Di Cicco, A.; Aquilanti, G.; Minicucci, M.; Filipponi, A.; Rybicki, J. *J. Phys.: Condens. Matter* **1999**, *11*, L43.
(31) Aquilanti, G.; Di Cicco, A.; Minicucci, M.; Filipponi, A.; Rybicki, J. *J. Synchrotron Radiat.* **1999**, *6*, 251.
(32) Di Cicco, A.; Taglienti, M.; Minicucci, M.; Filipponi, A. *Phys. Rev. B* **2000**, *62*, 12001.
(33) Rybicki, J.; Rybicka, A.; Witkowska, A.; Bergmański, G.; Di Cicco, A.; Minicucci, M.; Mancini, G. *J. Phys.:Condens. Matter* **2001**, *13*, 9781.
(34) Trapananti, A.; Di Cicco, A.; Minicucci, M. *Phys. Rev. B* **2002**, *66*, 14202.
(35) Di Cicco, A.; Minicucci, M.; Principi, E.; Witkowska, A.; Rybicki, J.; Laskowski, R. *J. Phys.: Condens. Matter* **2002**, *14*, 3365.
(36) Kuzmin, A.; Obst, S.; Purans, J. *J. Phys.: Condens. Matter* **1997**, *9*, 10065.
(37) Galoisy, L.; Delaye, J M.; Ghaleb, D.; Calas, G.; Le Grand, M.; Morin, G.; Ramos, A.; Pacaud, F. *Mater. Res. Soc. Symp. Proc.* **1998**, *506*, 133.
(38) Rossano, S.; Ramos, A.; Delaye, J.-M.; Filipponi, A.; Creux, S.; Brouder, C.; Calas, G. *J. Synchrotron Radiat.* **1999**, *6*, 247.
(39) Rossano, S.; Ramos, A.; Delaye, J.-M.; Creux, S.; Filipponi, A.; Brouder, C.; Calas, G. *Europhys. Lett.* **2000**, *49*, 597.
(40) Rossano, S.; Ramos, A. Y.; Delaye, J.-M. *J. Non-Cryst. Solids* **2000**, *273*, 48.
(41) Ferlat, G.; San Miguel, A.; Xu, H.; Aouizerat, A.; Blase, X.; Zuñiga, J.; Muñoz Sanjosé, V. *Phys. Rev. B* **2004**, *69*, 155202.
(42) Park, B.; Li, H.; Corrales, L. R. *J. Non-Cryst. Solids* **2002**, *297*, 220.
(43) Wallen, S. L.; Palmer, B. J.; Pfund, D. M.; Fulton, J. L.; Newville, M.; Ma, Y.; Stern, E. A. *J. Phys. Chem. A* **1997**, *101*, 9632.
(44) Wallen, S. L.; Palmer, B. J.; Fulton, J. L. *J. Chem. Phys.* **1998**, *108*, 4039.
(45) Fulton, J. L.; Hoffmann, M. M.; Darab, J. G.; Palmer, B. J.; Stern, E. A. *J. Phys. Chem. A* **2000**, *104*, 11651.
(46) Spångberg, D.; Hermansson, K.; Lindqvist-Reis, P.; Jalilehvand, F.; Sandström, M.; Persson, I. *J. Phys. Chem. B* **2000**, *104*, 10467.
(47) Jalilehvand, F.; Spångberg, D.; Lindqvist-Reis, P.; Hermansson, K.; Persson, I.; Sandström, M. *J. Am. Chem. Soc.* **2001**, *123*, 431.
(48) Sandström, M.; Persson, I.; Jalilehvand, F.; Lindqvist-Reis, P.; Spångberg, D.; Hermansson, K. *J. Synchrotron Radiat.* **2001**, *8*, 657.
(49) Merkling, P. J.; Muñoz Páez, A.; Martínez, J. M.; Pappalardo, R. R.; Sánchez Marcos, E. *Phys. Rev. B* **2001**, *64*, 12201.
(50) Merkling, P. J.; Muñoz Páez, A.; Sánchez Marcos, E. *J. Am. Chem. Soc.* **2002**, *124*, 10911.
(51) Okamoto, Y. *Nucl. Instrum. Methods Phys. Res. A* **2004**, *526*, 572.
(52) Campbell, L.; Rehr, J. J.; Schenter, G. K.; McCarthy, M. I.; Dixon, D. *J. Synchrotron Radiat.* **1999**, *6*, 310.
(53) Palmer, B. J.; Pfund, D. M.; Fulton, J. L. *J. Phys. Chem.* **1996**, *100*, 13393.
(54) (a) Rehr, J. J.; Albers, R. C.; Zabinsky, S. I. *Phys. Rev. Lett.* **1992**, *69*, 3397. (b) Newville, M.; Ravel, B.; Haskel, D.; Rehr, J. J.; Stern, E. A.; Yacoby, Y. *Physica B* **1995**, *208*−*209*, 154.
(55) Ankudinov, A. L.; Bouldin, C.; Rehr, J. J.; Sims, J.; Hung, H. *Phys. Rev. B* **2002**, *65*, 104107.
(56) Fulton, J. L.; Heald, S. M.; Badyal, Y. S.; Simminson, J. M. *J. Phys. Chem.* **2003**, *107*, 4688.
(57) Glezakou, V.-A.; Yongsheng, C.; Fulton, J. L.; Schenter, G. K.; Dang, L. X. *Theor. Chem. Acc.* **2005**, *214*, 54. Dang, L. X. *J. Phys. Chem.* **2002**, *106*, 10388.
(58) Dunning, T. H. *J. Chem. Phys.* **1989**, *90*, 1007.
(59) Feller, D.; Glendening, E. D.; Woon, D. E.; Feyereisen, M. W. *J. Chem. Phys.* **1995**, *103*, 3526.
(60) Woon, D. E.; Dunning, T. H. *J. Chem. Phys.* **1995**, *103*, 4572.
(61) Glendening, E. D.; Feller, D. *J. Phys. Chem.* **1996**, *100*, 4790.
(62) Kaupp, M.; Schleyer, P. v. R. *J. Phys. Chem.* **1992**, *96*, 7316.
(63) Xantheas, S. S. *J. Phys. Chem.* **1995**, *100*, 9703.
(64) Masamura, M. *J. Phys. Chem.* **2002**, *106*, 8925.
(65) Johnson, R. D. E., Benchmark; NIST Standard Database, 2005.
(66) Schmidt, M. W.; Baldridge, K. K.; Boatz, J. A.; Elbert, S. T.; Gordon, M. S.; Jensen, J. H.; Koseki, S.; Matsunaga, N.; Nguyen, K. A.; Su, S. J.; Windus, T. L.; Dupuis, M.; Montgomery, J. A. *GAMESS Program* **1993**, *14*, 1347.
(67) Dang, L. X.; Schenter, G. K.; Fulton, J. L. *J. Phys. Chem.* **2003**, *107*, 14119.
(68) Keese, R. G.; Castleman, A.W., Jr. *J. Phys. Chem. Ref. Data* **1986**, *15*(3), 1011.